JACS
JOURNAL OF THE AMERICAN CHEMICAL SOCIETY

Article

Synthesis and Characterization of the Most Active Copper ATRP Catalyst Based on Tris[(4-dimethylaminopyridyl)methyl]amine

Thomas G. Ribelli, Marco Fantin, Jean-Claude Daran, Kyle F. Augustine, Rinaldo Poli, and Krzysztof Matyjaszewski

J. Am. Chem. Soc., **Just Accepted Manuscript** • DOI: 10.1021/jacs.7b12180 • Publication Date (Web): 10 Jan 2018

ACS Publications

Journal of the American Chemical Society is published by the American Chemical Society. 1155 Sixteenth Street N.W., Washington, DC 20036

Synthesis and Characterization of the Most Active Copper ATRP Catalyst Based on Tris[(4-dimethylaminopyridyl)methyl]amine

Thomas G. Ribelli,[a◊] Marco Fantin,[a◊] Jean-Claude Daran,[b] Kyle F. Augustine,[a] Rinaldo Poli[b,c] and Krzysztof Matyjaszewski*[a]

[a]Department of Chemistry, Carnegie Mellon University, 4400 Fifth Avenue, Pittsburgh, PA 15213, United States
[b]CNRS, LCC (Laboratoire de Chimie de Coordination), Université de Toulouse, UPS, INPT, 205 Route de Narbonne, BP 44099, F-31077, Toulouse Cedex 4, France
[c]Institut Universitaire de France, 1, rue Descartes, 75231 Paris Cedex 05, France

ABSTRACT

The synthesis and characterization of tris[(4-dimethylaminopyridyl)methyl]amine ($TPMA^{NMe2}$) as a ligand for copper catalyzed atom transfer radical polymerization (ATRP) is reported. In solution, the $[Cu^{I}(TPMA^{NMe2})Br]$ complex shows fluxionality by variable temperature NMR, indicating rapid ligand exchange. In the solid-state, the $[Cu^{II}(TPMA^{NMe2})Br][Br]$ complex exhibits a slightly distorted trigonal bipyramidal geometry (τ = 0.89). The UV-Vis spectrum of $[Cu^{II}(TPMA^{NMe2})Br]^{+}$ salts is similar to those of other pyridine-based ATRP catalysts. Electrochemical studies of $[Cu(TPMA^{NMe2})]^{2+}$ and $[Cu(TPMA^{NMe2})Br]^{+}$ showed highly negative redox potentials ($E_{1/2}$ = -302 mV and -554 mV vs. SCE, respectively), suggesting unprecedented ATRP catalytic activity. Cyclic voltammetry (CV) in the presence of methyl 2-bromopropionate (MBrP; acrylate mimic) was used to determine activation rate constant $k_a = 1.1 \times 10^6$ $M^{-1}s^{-1}$, confirming the extremely high catalyst reactivity. In the presence of the more active ethyl α-bromoisobutyrate (EBiB; methacrylate mimic), total catalysis was observed and an activation rate constant $k_a = 7.2 \times 10^6$ $M^{-1}s^{-1}$ was calculated with values of $K_{ATRP} \approx 1$. ATRP of methyl acrylate showed a well-controlled polymerization using as little as 10 ppm of catalyst relative to monomer while side reactions such as Cu^{I} catalyzed radical termination (CRT) could be suppressed due to the low concentration of L/Cu^{I} at a steady-state.

INTRODUCTION

Atom transfer radical polymerization (ATRP) has gained widespread use due to its easy setup, tolerance to functional groups, mild conditions and wide range of applications.[1-4] Since its inception in 1995, when stoichiometric amounts of air-sensitive Cu^{I} relative to alkyl halide initiator were used,[5] many advances have been made to improve the efficiency of this polymerization system.[6] The development of new operating techniques such as initiators for continuous activator regeneration (ICAR) ATRP[7-8], activators regenerated by electron transfer

(ARGET) ATRP[9-11], supplemental activators and reducing agents (SARA) ATRP[12] as well as photoATRP[13-17], *e*ATRP[18] and most recently mechanoATRP[19-20] have allowed polymerizations to be conducted using ppm levels of catalyst relative to monomer.

As shown in **Scheme 1**, the control in ATRP is achieved via a reversible redox equilibrium between a L/$Cu^{I/II}$ couple where L signifies a multidentate nitrogen-based ligand. L/Cu^{I} activates a (macro)alkyl halide chain end, resulting in the L/Cu^{II}-X deactivator and a carbon-based radical,[21] which propagates by adding to monomer before being trapped by the L/Cu^{II}-X deactivator, regenerating the L/Cu^{I} species and the dormant polymer chain.[4] To control the polymerization,[22] this equilibrium (K_{ATRP}) should lie on the dormant side to diminish the concentration of radicals and retain chain-end functionality (CEF). K_{ATRP} can be expressed as the ratio of activation (k_a) to deactivation (k_d) rate constants and can be tuned over 8-orders of magnitude[23] based on temperature, pressure, solvent,[24-25] polymer chain-end,[26] and choice of catalyst.[23] In order to reach even lower catalyst loadings or to polymerize less active monomers such as vinyl acetate (VAc),[27] higher values of K_{ATRP} must be achieved.

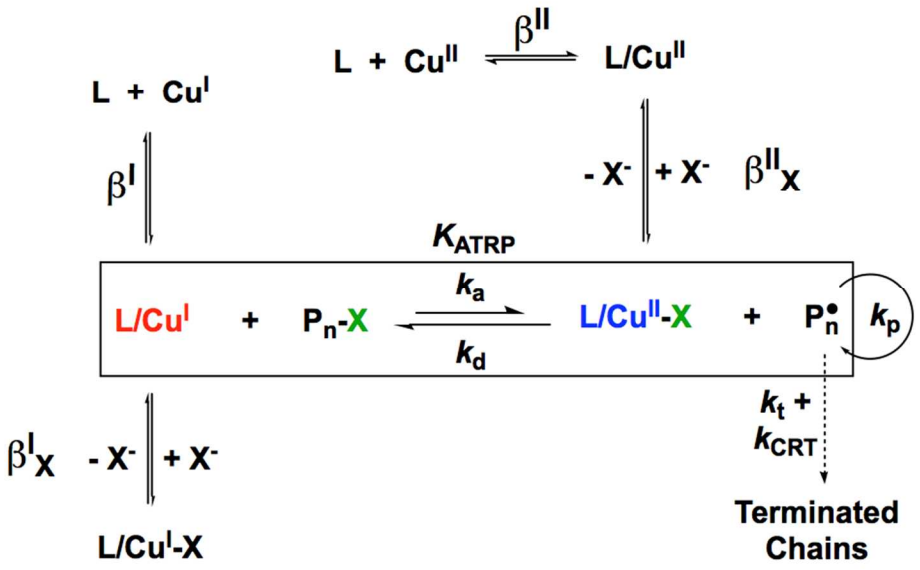

Scheme 1 Mechanism of ATRP (boxed) and equilibria involving association of ligand (β^m) and halide (β^m_x) to either the Cu^{I} (m = I) or Cu^{II} (m = II) ion.

One simple way to tune ATRP is by changing the coordination sphere of copper. Over the years, rational ligand design has allowed for the understanding of how the catalyst structure affects reactivity. The activity of the catalyst in ATRP correlates with ligand denticity,

nature of the N-donor atom and electron donating ability through the coordinating nitrogen atom(s).[28] Indeed, a linear correlation between the redox potential ($E_{1/2}$) and ln(K_{ATRP}) has been established where a more negative $E_{1/2}$ results in a larger value of K_{ATRP}.[29] This strong correlation allows for the prediction of new catalysts' activity based solely on their redox potential. The activity of a catalyst can also be further assessed by comparing the stability constants (binding constants), β, of the L/Cu^{I} and L/Cu^{II} complexes since K_{ATRP} scales with the β^{II}/β^{I} ratio, as shown in **Scheme 1**. While both β^{II} and β^{I} should be large, $\beta^{II} > \beta^{I}$ in order to provide a thermodynamic driving force for alkyl halide activation.[29] Indeed, β^{I} values are rather constant but β^{I} values change significantly with the ligand structures.[30]

To date, the most active ATRP catalyst has used the ligand tris[((4-methoxy-2,5-dimethyl)-2-pyridyl)methyl]amine (TPMA*^{3}) which has three electron donating groups on each pyridine ring.[31-32] This led to a catalyst that is 5 million times more active than the seminal catalytic system employing the 2,2'-bipyridine (bpy) ligand and 1000 times more active than the commonly used tris(pyridylmethyl)amine (TPMA) ligand (**Scheme 2**).

According to Hammett parameters, using the even more electron donating dimethyl amino (–NMe_2) group should further increase the catalyst activity as already observed for bpy derivatives.[33] Therefore, we have considered using tris[(4-dimethylamino-2-pyridyl)methyl]amine (TPMA^{NMe2}) ligand as shown in **Scheme S1**.[34-36] This ligand was previously reported by Karlin *et al* where the [Cu^{I}(TPMA^{NMe2})]$^{+}$ complex was used as an oxygen activation catalyst to mimic various copper containing enzymes[37-38] such as amine oxdiases,[39] multicopper oxidases[40] (MCOs) and tyrosinases[41] as well as to study this complex's interactions with carbon monoxide.[42] This new Cu-based ATRP catalyst with TPMA^{NMe2}, in both relevant oxidation states, has been characterized in solution and the solid state and utilized in ATRP systems with low catalyst loadings (down to 10 ppm) and was shown to exhibit unprecedented reactivity with alkyl halides.

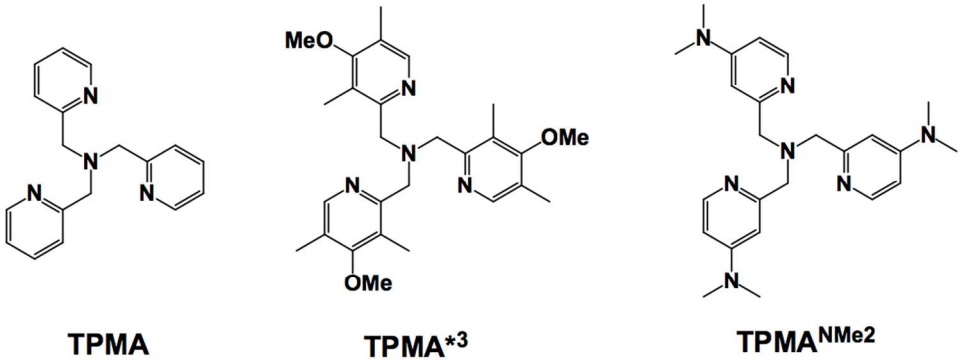

Scheme 2 Structure of the ligands used in this study.

RESULTS AND DISCUSSION

TPMA^{NMe2} was prepared by a procedure slightly modified from that used by Karlin *et al*[34] (**Scheme S1)**. The synthesis of 2-hydroxymethyl-4-dimethylaminopyridine *(***2; Scheme S1***)* was conducted as previously published by Comba *et al*.[35] The synthesis of 2-phthalimidomethyl-4-chloropyridine (**5; Scheme S1**) was conducted as previously published by our group.[31] 2-Aminomethyl-4-dimethylpyridine (**6; Scheme S1**) was synthesized directly from a basic workup of 2-phthalimidomethyl-4-dimethylaminopyridine. It should be noted that it is very important to use chemical resistant O-Ring (ACE glass # 7855-813) for reactions using high pressure tubes. The ligand has been characterized by $^{1}H/^{13}C$ NMR and ESI-MS which confirmed the predicted structure.

Variable Temperature NMR of Cu^{I} complexes

It has been previously shown that L/Cu^{I} complexes with multidentate pyridine-based ligands can undergo fast ligand exchange in the presence of excess ligand relative to Cu^{I}.[43] The solution prepared by addition of TPMA^{NMe2} to CuBr was studied by variable temperature NMR, as shown in **Figure 1**.

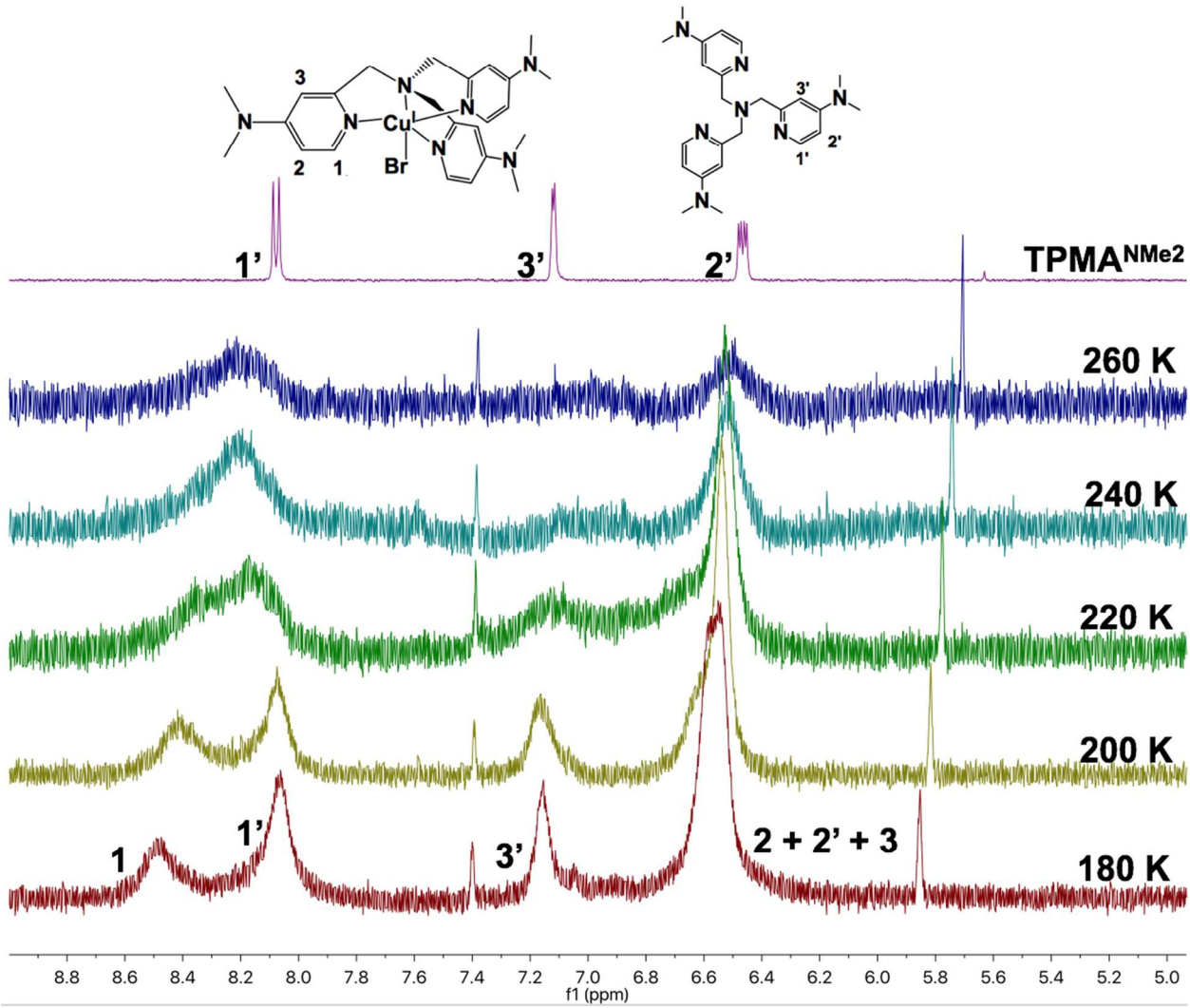

Figure 1 Variable temperature ^{1}H NMR of the aromatic region of the free TPMA^{NMe2} ligand and its CuBr complex at the molar ratio $[CuBr]_0$:$[TPMA^{NMe2}]_0$ = 1:3 in d_6-acetone.

Upon reacting equimolar amounts of TPMA^{NMe2} and CuBr in d_6-acetone, the reaction initially turned to a pale-yellow color, common for Cu^{I} complexes coordinated by pyridinic ligands. However, upon stirring, the reaction mixture turned green along with a dark precipitate indicative that the [Cu^{I}(TPMA^{NMe2})Br] complex underwent disproportionation to [Cu^{II}(TPMA^{NMe2})Br][Br] and Cu^{0} + TPMA^{NMe2}. Typically, unsubstituted TPMA shows little to no disproportionation. The position of the disproportionation equilibrium, $K_{Disp,LCu}$, depends on the relative stability of LCu^{II} compared LCu^{I}. Since TPMA^{NMe2} stabilizes Cu^{II} much more than TPMA, disproportionation is possible. This is especially true in a disproportionating solvent such as

acetone, which is polar and coordinates weakly to Cu^{I}.[29] To suppress disproportionation and reform the [Cu^{I}(TPMA^{NMe2})Br] complex, 2 additional equivalents of TPMA^{NMe2} were added.[44] Indeed, upon further stirring for 30 minutes, the reaction regained its yellow color and the Cu^{0} particles were no longer visible.

The ^{1}H NMR spectrum shows significant broadening of the aromatic peaks upon complexation, which has been previously been shown for other Cu^{I} complexes.[45-47] This broadening indicates a fast exchange between free and coordinated ligand. Upon decreasing the temperature to 240 K, the peaks attributed to coordinated and uncoordinated ligand began to resolve due to the slower rate of exchange. At 180 K, two distinct peaks were observed at 8.05 and 8.5 ppm, attributed to free and coordinated ligand, respectively.[43, 48-51] The peaks became narrower at lower temperature but were broader than those of previously published TPMA-based Cu^{I} complexes at 180 K. This could be due to the presence of small amounts of paramagnetic Cu^{II} formed from disproportionation and plausible self-exchange between the Cu^{II} and Cu^{I} complexes. This cannot be avoided due to the disproportionating nature of acetone and the highly reactive [Cu^{I}(TPMA^{NMe2})]$^{+}$ complex. Although the variable temperature NMR spectra indicate a significant amount of ligand exchange, the total amount of uncoordinated Cu is extremely low due to the large stability constants, β^{I}, as has been previously observed for substituted TPMA ligands.[43]

Structural Studies of Cu^{II} Deactivator Complex The [Cu^{II}(TPMA^{NMe2})Br]$^{+}$ complex was synthesized and crystallized as reported in the Supporting Information. The resulting molecular structure is presented in **Figure 2** with selected bond distances and angles summarized in **Table 1**.

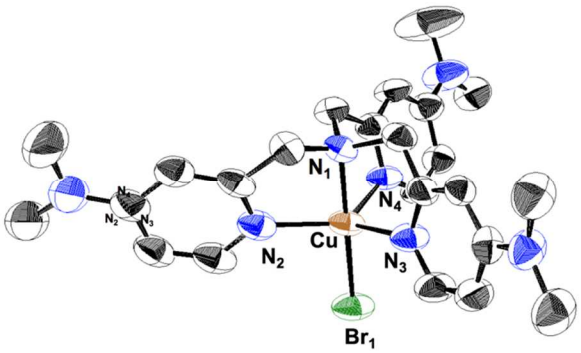

Figure 2 Molecular structure of $[Cu^{II}(TPMA^{NMe2})Br][Br]$ shown (left) with 50% probability displacement ellipsoids. H atoms, counter Br^- anion and solvent molecules have been omitted for clarity.

The $[Cu^{II}(TPMA^{NMe2})Br]^+$ cation is in a slightly distorted trigonal bipyramidal geometry, indicated by a structural parameter τ = 0.89 (τ = 1.00 for trigonal bipyramidal). Coordination of the tetradentate ligand occurs through three substituted pyridinic nitrogen atoms in the equatorial plane (N_{eq}) and a central anchoring aliphatic nitrogen in the axial plane (N_{ax}). The N_{ax}-Cu-N_{eq} bond angles are all slightly smaller than 90° which is consistent with a previously reported cupric aqua adduct,[36] $[Cu^{II}(TPMA^{NMe2})(H_2O)]^{2+}$. The similar N_{ax}-Cu-N_{eq} angles between the two complexes, although with differently sized axial ligands (Br^- vs. H_2O), suggests these deviations from 90° are most likely due to the natural bite of the ligand as opposed to steric repulsion from the axial ligand. The previously reported[42] cuprous carbonyl adduct, $[Cu^{I}(TPMA^{NMe2})(CO)]^+$, showed a Cu^{I}-N_{ax} bond distance of 2.446 Å which is significantly elongated compared to the Cu^{II}-N_{ax} bond distance of 2.05 Å presented in this study. Although the two complexes cannot be directly compared due to the difference in axial ligand, Cu-N_{ax} bond elongation upon reduction of Cu^{II} to Cu^{I} has been observed in other TPMA-based complexes.[52] This is attributed to Cu^{II} preferring a 5-coordinate environment while the reduced Cu^{I} ion prefers 4-coordinate geometries.[53] Thus, the Cu^{I}-N_{ax} bond is elongated to a non-bonding distance forming a distorted tetrahedral geometry. Furthermore, as shown in **Figure S5**, the crystal structure is stabilized by π–π stacking interactions between substituted pyridine rings as well as weak C-H---Br (2.84 Å) interactions.

Table 1 Selected Bond Distances and Angles of Relevance for L/Cu^{II}-Br Deactivator Species[a]

	$[Cu^{II}(TPMA)Br][Br]$[b]	$[Cu^{II}(TPMA*^{3})Br][Br]$[c]	$[Cu^{II}(TPMA^{NMe2})Br][Br]$[d]
Cu-$N1_{ax}$	2.040(3)	2.028(3)	2.047(3)
Cu-$N2_{eq}$	2.073(15)	2.059(3)	2.051(2)
Cu-$N3_{eq}$	2.073(15)	2.149(3)	2.108(3)
Cu-$N4_{eq}$	2.073(15)	2.044(3)	2.046(3)
Cu-Br_1	2.384(6)	2.3740(5)	2.3898(6)
N_1-Cu-N_2	80.86(5)	81.07(12)	80.59(10)
N_1-Cu-N_3	80.86(5)	82.81(12)	80.60(10)

N_1-Cu-N_4	80.86(5)	79.82(11)	81.42(10)
N_2-Cu-N_3	117.53(3)	132.39(12)	126.78(10)
N_2-Cu-N_4	117.53(3)	115.63(12)	116.34(10)
N_3-Cu-N_4	117.53(3)	104.99(12)	109.40(10)
N_1-Cu-Br_1	180.00(5)	178.33(9)	179.89(9)
N_2-Cu-Br_1	99.14(5)	100.99(8)	98.59(8)
N_3-Cu-Br_1	99.14(5)	98.35(8)	99.49(7)
N_4-Cu-Br_1	99.14(5)	97.27(8)	99.32(7)
τ[e]	1.0	0.77	0.89

[a]Bond lengths are given in angstroms (Å) and angles in degrees (°). [b]From Ref 51. [c]From Ref 42. [d]This work. [e]τ parameter is calculated as $\tau = (\phi_1 - \phi_2)/60$, where ϕ_1 and ϕ_2 are the largest (N_1-Cu-Br_1) and second largest (N_2-Cu-N_3) bond angles, $\tau = 1$ (trigonal bipyramidal geometry), and $\tau = 0$ (square pyramidal geometry).

Solution Studies of Cu^{II} Complexes The UV-Vis-NIR spectra were obtained using $CuBr_2$ to form $[Cu^{II}(TPMA^{NMe2})Br]^+$ and also $Cu(OTf)_2$ to form $[Cu^{II}(TPMA^{NMe2})(MeCN)]^{2+}$, since the OTf^- anion coordinates very weakly to the Cu^{II} center in solution. As shown in **Figure 3A**, two d→d transitions are observed in the NIR and visible region at 1038 and 776 nm for the $[Cu^{II}(TPMA^{NMe2})Br]^+$ and 980 and 725 nm for the $[Cu^{II}(TPMA^{NMe2})(MeCN)]^{2+}$ complex, respectively. These two transitions are typical of d^9 Cu^{II} possessing trigonal bipyramidal geometry and are attributed to $d_{xz} \approx d_{yz} \rightarrow d_{z2}$ and to $d_{x2-y2} \approx d_{xy} \rightarrow d_{z2}$.[54-55] A ligand to metal charge transfer (LMCT) band is apparent in both complexes, centered around 425 and 395 nm for $[Cu^{II}(TPMA^{NMe2})Br]^+$ and $[Cu^{II}(TPMA^{NMe2})(MeCN)]^{2+}$, respectively. The absorption spectra of these two complexes are consistent with previously published results for many ATRP deactivator complexes presenting trigonal bipyramidal geometry.[43, 56]

A sample of $[Cu^{II}(TPMA^{NMe2})Br][Br]$ crystals was also investigated, after dissolution into a dichloromethane (DCM)/toluene mixture, by X-Band EPR spectroscopy at 120 K as shown in **Figure 3B**. The spectrum revealed a pattern and g/A parameters rather close to those of the related $[Cu^{II}(TPMA)Br]^+$ complex.[57] On the other hand, a rather uninformative cubit tensor at g = 2.123 and a linewidth of ca. 110 G without observable copper hyperfine coupling was observed in pure MeCN or pure DCM as shown in **Figure S4**.

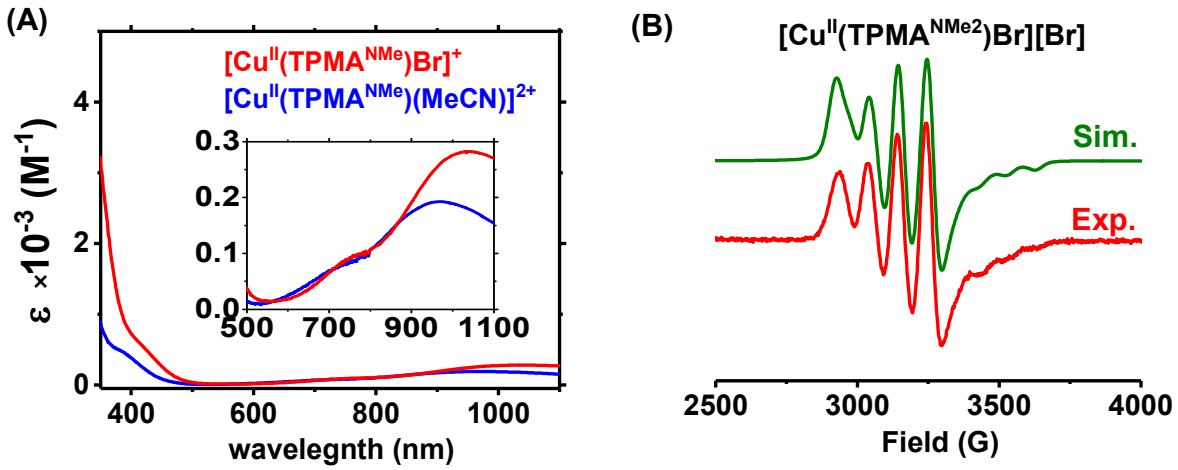

Figure 3 A) Absorption spectra of the $[Cu^{II}(TPMA^{NMe2})Br]^+$ deactivator complex (red) and $[Cu^{II}(TPMA^{NMe2})(MeCN)]^{2+}$ complex (blue) in MeCN. $[CuX_2]_0$ = 1 mM (X = Br^- or OTf^-) and B) Experimental (red) and simulated (green) X-band EPR spectra of the $[Cu^{II}(TPMA^{NMe2})Br][Br]$ complex in a 1:1 mixture of DCM:toluene recorded at 120K (g_1 = 2.173, A_1 = 255.3 MHz, g_2 = 2.198, A_2 = 336.5 MHz, g_3 = 1.95, A_3 = 260.1 MHz).

Thermodynamic Parameters As noted above, one method to determine catalyst activity in ATRP is by measuring the stability constants, β^{I} and β^{II}, for the L/Cu^{I} and L/Cu^{II} complexes.[43] The redox potential of the $[Cu(L)]^{2+}$ complex gives the β^{II}/β^{I} ratio as shown in **Eq 1**, where $E^{\circ}_{Cu^{2+}/Cu^{+}}$ and $E^{\circ}_{LCu^{II}/LCu^{I}}$ represent the standard redox potential of solvated Cu and the ligated Cu species, respectively.[58] Furthermore, according to **Eq 2**, it is also possible to obtain the ratio $\beta^{II}_{X,app}/\beta^{I}_{X,app}$ electrochemically, where $\beta^{II}_{X,app}$ and $\beta^{I}_{X,app}$ are the apparent equilibrium constants of halide association to ligated copper, L/Cu^{II}–X or L/Cu^{I}–X, respectively.[43] $\beta^{II}_{X,app}$ considers that addition of X^- do not change the original β^{I} and β^{II} values. For efficient deactivation, β^{II}_{X} values must be high. Values of β^{I}_{X} should be low, since the $[Cu^{I}(L)Br]$ is an inefficient activator in ATRP.[59]

$$\ln\frac{\beta^{I}}{\beta^{II}} = \frac{F}{RT}\left(E^{o}_{Cu^{2+}/Cu^{+}} - E^{o}_{LCu^{II}/LCu^{I}}\right) \qquad \textbf{(Eq. 1)}$$

$$\ln\frac{\beta^{II}_{X,app}}{\beta^{I}_{X,app}} = \frac{F}{RT}\left(E^{o}_{LCu^{II}/LCu^{I}} - E^{o}_{LCu^{II}-X/LCu^{I}-X}\right) \qquad \textbf{(Eq. 2)}$$

As shown in **Figure 4**, both the $[Cu(TPMA^{NMe2})(MeCN)]^{2+}$ and $[Cu(TPMA^{NMe2})Br]^{+}$ complexes exhibit a reversible redox wave at $E_{1/2}$ = -302 mV and -554 mV vs. SCE, respectively, representing the most reducing ATRP catalysts to date. Separation between the anodic and cathodic peaks is ca. 60 mV at a scan rate of 0.2 V s^{-1}, indicating good reversibility. Increasing the scan rate results in the expected increase in current; peak separation also increases, revealing a quasi-reversible nature of the electron transfer. This shows that the $TPMA^{NMe2}$ ligand is able to sufficiently stabilize the electrochemically generated Cu^{I}, and indicates that these complexes have small rearrangement energies between the $Cu^{I/II}$ oxidation states. Using **Eq 1**, the β^{II}/β^{I} ratio was calculated as 1.1 x 10^{23} (**Table 2**) which is 1500 times larger than the previously reported value for the tris(2-dimethylaminoethyl)amine (Me_6TREN) complex in MeCN.[58] This large increase may be either due to a more stabilized Cu^{II} or a destabilized Cu^{I}. However, it was previously shown[43] that stability constants for Cu^{I} were similar using variously substituted pyridine-based ligands in DMF.[30]

Upon introduction of coordinating bromide anions, the complex $[Cu(TPMA^{NMe2})Br]^{+}$ is formed, and the redox potential shifts by -252 mV to give $E_{1/2}$ = -554 mV vs. SCE. K_{ATRP} increases roughly one order of magnitude for every 59 mV shift of redox potential,[26] indicating K_{ATRP} should be approximately 140,000 times greater relative to the unsubstituted TPMA-based catalyst, which has $E_{1/2}$ = -240 mV vs. SCE,[46] and >10^9 times greater than the original bpy catalyst, which has $E_{1/2}$ = +30 mV vs. SCE.[60] Furthermore, using **Eq. 2**, the $\beta^{II}_{X,app}/\beta^{I}_{X,app}$ ratio was calculated to be 1.8 x 10^4, similar to that of other TPMA-based ligands in MeCN.[43]

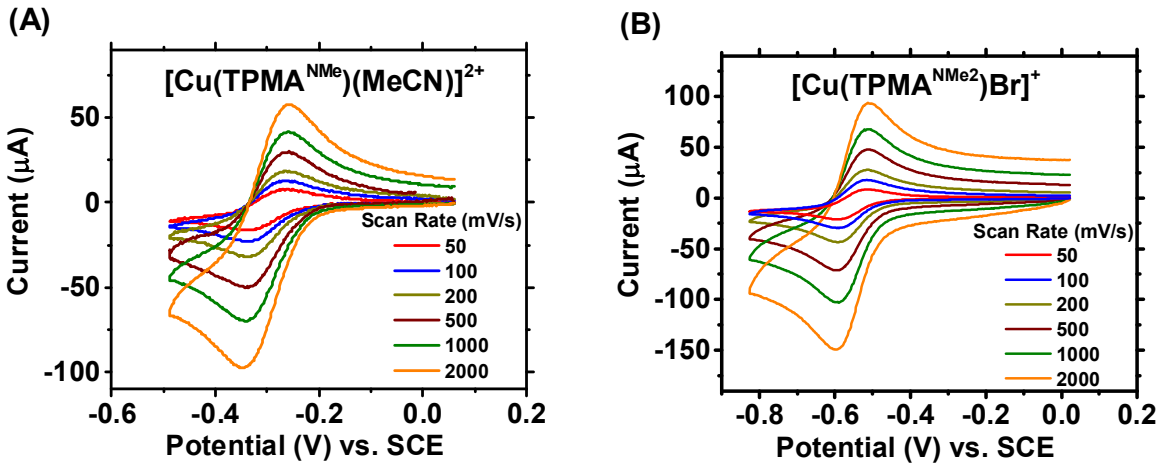

Figure 4 Cyclic voltammograms of (A) 1 mM $[Cu(TPMA^{NMe2})(MeCN)]^{2+}$ and (B) 1 mM $[Cu(TPMA^{NMe2})Br]^{+}$ + 20 mM Et_4NBr in dry MeCN at different scan rates using Et_4NBF_4 as a supporting electrolyte and glassy carbon working electrode; $[L/Cu^{II}]_0$ = 1 mM.

$$K_{\text{disp,LCu}} = \frac{[\text{LCu}^{\text{II}}]_{\text{eq}}[\text{L}]_{\text{eq}}}{[\text{LCu}^{\text{I}}]_{\text{eq}}^{2}} \quad \textbf{(Eq. 3)}$$

$$\frac{\beta^{\text{II}}}{(\beta^{\text{I}})^{2}} = \frac{K_{\text{disp,LCu}}}{K_{\text{disp,Cu}}} \quad \textbf{(Eq. 4)}$$

Since cyclic voltammetry can only provide the β^{II}/β^{I} ratio, further analysis was carried out to estimate the individual β values. We previously reported[43] on the disproportionation equilibrium allowing for the calculation of $\beta^{II}/(\beta^{I})^2$, as shown in **Eq's 3 & 4**, where $K_{disp,LCu}$ and $K_{disp,Cu}$ are the equilibrium constants of disproportionation for ligated and solvated copper, respectively.[43] The determination of the disproportionation equilibrium, when coupled with electrochemical measurements, allows for the calculation of individual stability constants.

Analysis of $K_{disp,LCu}$ is difficult in MeCN due to the highly comproportionating nature of this solvent, i.e. very small values of $K_{disp,}$. In fact, values of $K_{disp,Cu}$ for the solvated Cu^{I} complex in acetonitrile have previously been estimated on the order of 10^{-21}.[61] Therefore, it was only possible to estimate a limit of $K_{disp,LCu} < 1.0 \times 10^{-4}$. Nonetheless, using this value the lower limits of β^{II} and β^{I} as 3.5×10^{29} and 1.9×10^{6} were estimated, respectively. These values, although likely underestimated due to uncertainty of $K_{disp,LCu}$, are in good agreement with previously reported values for other ATRP catalysts.[43, 58] All thermodynamic parameters obtained in this study, as well as for TPMA and TPMA*[3]-based complexes, are summarized in **Table 2**. It should be noted that values of β^{I} are significantly limited by unattainable values of $K_{disp,LCu}$ in MeCN.

Table 2 Thermodynamic Properties of the $[Cu(L)(MeCN)]^{2+}$ and $[Cu(L)Br]^{+}$ Complexes in MeCN (L = TPMA, TPMA*[3], $TPMA^{NMe2}$)

	TPMA	TPMA*[3]	$TPMA^{NMe2}$
[a]$E_{1/2,Cu}$	1.06	1.06	1.06
$E_{1/2,LCu}$	-0.030[c]	-0.177[b]	-0.302
$E_{1/2,LCuBr}$	-0.240	-0.420	-0.554
$E_{1/2,Cu}$-$E_{1/2,LCu}$	1.090	1.237	1.362

$E_{1/2,LCu}$-$E_{1/2,LCuBr}$	0.210	0.243	0.252
[d]$K_{Disp,Cu}$	1.0×10^{-21}	1.0×10^{-21}	1.0×10^{-21}
[e]$K_{Disp,LCu}$	$<1.0 \times 10^{-4}$	$<1.0 \times 10^{-4}$	$<1.0 \times 10^{-4}$
β^{II}/β^{I}	2.7×10^{18}	8.1×10^{20}	1.1×10^{23}
$\beta^{II}/(\beta^{I})^2$	$<1.0 \times 10^{17}$	$<1.0 \times 10^{17}$	$<1.0 \times 10^{17}$
β^{II}	$>7.1 \times 10^{19}$	$>6.6 \times 10^{24}$	$>1.1 \times 10^{29}$
β^{I}	$>2.7 \times 10^{1}$	$>8.1 \times 10^{3}$	$>1.1 \times 10^{6}$
$\beta^{II}_{X,app}/\beta^{I}_{X,app}$	5.3×10^{3}	1.3×10^{4}	5.3×10^{3}
[f]K_{ATRP}	$\approx 10^{-5}$	$\approx 10^{-3}$	$\approx 10^{-1}$
k_a (MBrP)	2.2×10^{2} [g]	8.4×10^{3} [h]	1.1×10^{6}

Redox potentials in V vs. SCE; k_a in $M^{-1}s^{-1}$. [a]Taken from literature[62]. [b]Taken from Ref[43], [c]Taken from Ref[46] using the conversion factor $E^o(Fc^+/Fc)$ = 0.390 V vs. SCE. [d]From Ref[61] [e]Experimental limiting value of $K_{Disp,LCu}$. [f]Estimated for acrylates based on value of $E_{1/2,LCuBr}$ and the trend of $E_{1/2}$ vs. K_{ATRP}[43] [g]From Ref[63] [h]From Ref[31].

Assessment of ATRP Activity

The ability of L/Cu^{I} complexes to activate (macro)alkyl halide bonds is paramount to the success of an ATRP system. The bond dissociation free energy (BDFE) of a C-X (X = Cl or Br) has been correlated to values of K_{ATRP} via DFT.[21, 27] Generally, the activation reaction is faster (larger values of k_a) if the resulting radical is more stabilized either through steric or resonance effects.

Electrochemistry is a useful tool in determining kinetic parameters in ATRP. The use of a rotating disk electrode allowed for measurement of k_a and K_{ATRP} for systems with moderately high activity ($k_a < 10^4$). For more active processes such as in aqueous media[64] and systems involving highly active catalysts[65], cyclic voltammetry of copper complexes under catalytic conditions (in the presence of RX) can be used to obtain k_a.[65-67] k_a is obtained from the current enhancement or degree of catalysis defined as $I_p/I_{p,0}$, where I_p and $I_{p,0}$ stand for the cathodic peak current of the catalyst measured in the presence and absence of initiator, respectively (**Figure 5B**). The procedure is described in the supporting information.

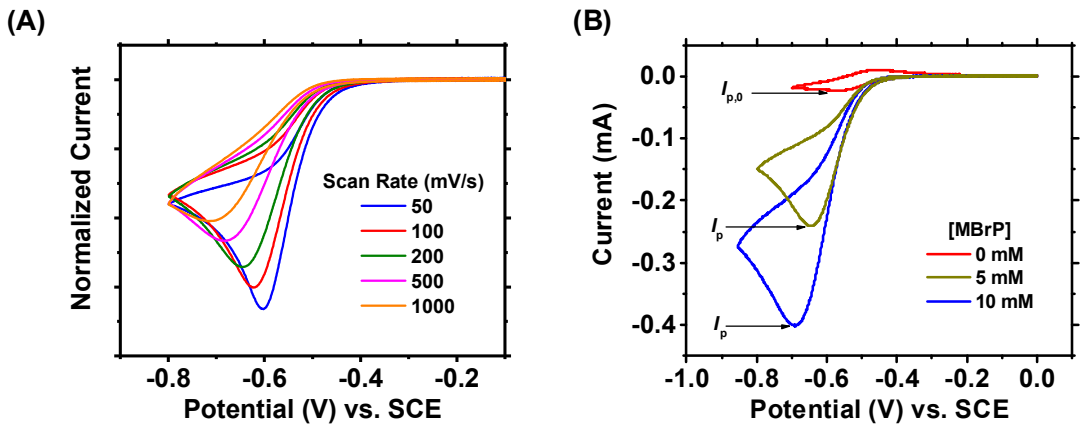

Figure 5 Cyclic voltammograms of $[Cu(TPMA^{NMe2})Br]^+$ in the presence of methyl 2-bromopropionate (MBrP; acrylate mimic) at (A) varying scan rates and (B) different $[MBrP]_0$ in MeCN at scan rate 0.2 V s^{-1} at room temperature. In (A) current was normalized by dividing by square root of the scan rate. $[MBrP]_0$:$[TPMA^{NMe2}]_0$:$[CuBr_2]_0$:$[TEMPO]_0$ = 0-10:1:1:10; $[CuBr_2]_0$ = 1 mM.

As shown in **Figure 5A**, cyclic voltammetry of the $[Cu(TPMA^{NMe2})Br]^+$ complex was conducted in the presence of methyl 2-bromopropionate (MBrP) and TEMPO. Here, MBrP acted as a small molecule model of acrylate chain-end, while TEMPO was used as a radical trap to prevent the deactivation reaction. The dramatic increase in $I_p/I_{p,0}$, as the scan rate decreased, is consistent with previous reports.[65, 68] The absence of an oxidation peak indicates that the electrochemically generated Cu^I was completely consumed in the activation of MBrP, showing the high activity of this catalyst in the activation of acrylates. As shown in **Figure S7**, cyclic voltammetry under catalytic conditions gave a rate coefficient of activation, k_a, of (1.1 ± 0.4) x 10^6 M^{-1} s^{-1}, which is the largest value reported for this initiator with copper-based ATRP catalysts. As will be shown later, values of k_d were calculated to be 5 x 10^7 $M^{-1}s^{-1}$. Thus, K_{ATRP} was estimated on the order of 10^{-1}. This value is consistent with that estimated from the redox potential (**Table 2**, K_{ATRP} = 1.0 x 10^{-1}). This also indicates that deactivation for so active and reducing complexes is still very efficient. These preliminary studies further indicate that this new complex is the most active copper-based ATRP catalyst to date.

Figure 6A shows cyclic voltammetry of $[Cu(TPMA^{NMe2})Br]^+$ in the presence of more active ethyl α-bromoisobutyrate (EBiB; methacrylate mimic). With $[EBiB]_0$ >> $[Cu^{II}(TPMA^{NMe2})Br]_0$ a large increase of the cathodic current and complete disappearance of the anodic peak was observed, similar to the voltammograms in the presence of the less active

MBrP. Cyclic voltammetry under catalytic conditions gave k_a = (7.2 ± 2.0) x 10^6 $M^{-1}s^{-1}$ indicating that K_{ATRP} approaches unity. However, at a ratio of $[Cu^{II}(TPMA^{NMe2})Br]_0$:$[EBiB]_0$ = 1, an interesting cyclic voltammogram was observed where the cathodic wave splits into two peaks (**Figure 6B**). This particular phenomenon is attributed to "total catalysis", which is usually found for extremely efficient catalysts with rate constants for bimolecular reactions > 10^6 M^{-1} s^{-1}.[69] Indeed, in this case, only an infinitesimal amount of L/Cu^I is required for the complete reduction of RBr, giving a first irreversible peak at $E > E_{1/2,LCuBr}$ due to the very fast catalytic reduction of EBiB. On the other hand, the electrochemical reduction of $[Cu(TPMA^{NMe2})Br]^+$ is still reversible since the majority of the catalyst is not involved in the electrocatalytic process. Overall, these results show the extreme reactivity of $[Cu(TPMA^{NMe2})Br]^+$, which can be used in ATRP with unprecedentedly low ppm concentrations.

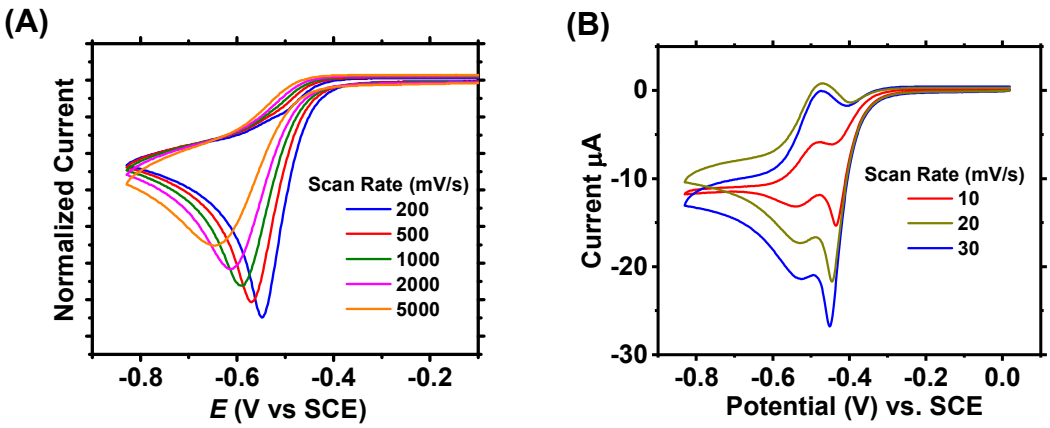

Figure 6. Cyclic voltammograms of 1 mM $[Cu(TPMA^{NMe2})Br]^+$ in the presence of ethyl α-bromoisobutyrate (EBiB; methacrylate mimic) at (A) 5 mM (B) 1 mM concentration in MeCN at at room temperature. In (A) current was normalized by dividing by square root of the scan rate. $[EBiB]_0$:$[TPMA^{NMe2}]_0$:$[CuBr_2]_0$:$[TEMPO]_0$ = 1-5:1:1:10.

Low ppm ATRP of Acrylates

To assess the efficiency of the $[Cu(TPMA^{NMe2})Br]^+$ catalyst, various forms of ATRP with activator regeneration were conducted. First, ICAR ATRP was conducted at catalyst loadings ranging from 10 to 100 ppm relative to monomer with 2,2'-azobis(2-isobutyronitrile) (AIBN) as radical initiator.[70] As shown in **Figure 7**, linear semi-logarithmic plots vs. time were observed at all catalyst loadings. This is consistent with previously established ICAR kinetics with bimolecular termination for which the amount of catalyst does not change the rate of polymerization as

shown in **Eq 5,** where f is initiator efficiency of AIBN, k_{azo} is the decomposition rate coefficient and k_t is the rate coefficient of radical-radical termination.[71-72]

$$[R^{\bullet}] = \sqrt{\frac{f k_{azo}[AIBN]}{k_t}} \quad \textbf{(Eq. 5)}$$

$$[R^{\bullet}] = \frac{f k_{azo}[AIBN]}{k_{CRT}^{app}[Cu^{I}]} \quad \textbf{(Eq. 6)}$$

After 4 hours, >90% conversion was achieved for all reactions with a linear increase of molecular weights with conversion, typical of a well-controlled polymerization. While the rate of polymerization was unaffected by the initial amount of catalyst, molecular weight distributions gradually broadened upon decreasing catalyst concentration (**Figure S9**). This is attributed to decreased rate of deactivation relative to propagation. Although the initial amount of catalyst does not affect the rate of polymerization, at lower catalyst loadings there is less deactivator complex to reversibly trap radicals. This causes more monomer additions per activation cycle and thus a broadening of the molecular weight distribution. (cf. **Eq. 7**)

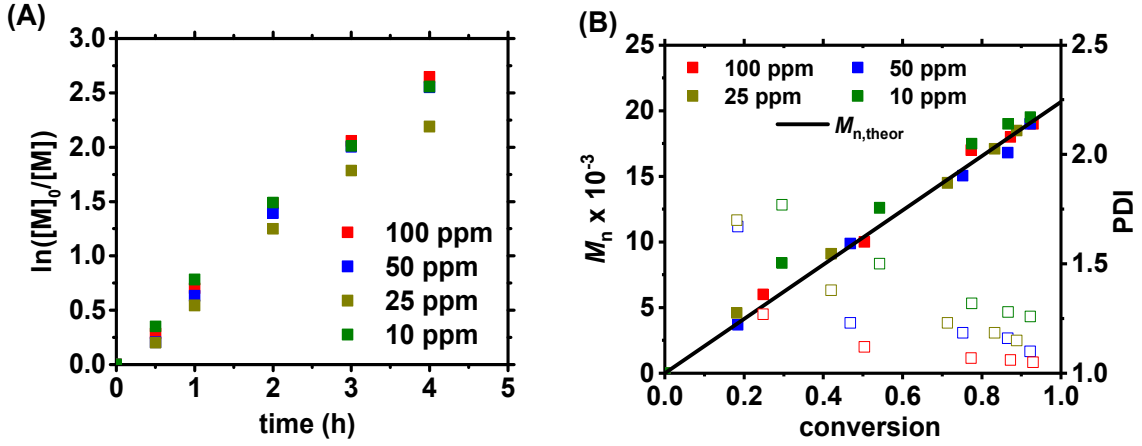

Figure 7 A) Semi-logarithmic plots and B) M_n and $Đ$ vs. conversion for the ICAR ATRP of *n*-butyl acrylate (BA) at different $[Cu^{II}(TPMA^{NMe2})Br][Br]$ loadings under the initial conditions $[BA]_0:[EBiB]_0:[L/CuBr_2]_0:[TPMA^{NMe2}]_0:[AIBN]_0$ = 160:1:0.016-0.0016:0.2 in anisole at 60 °C; catalyst loadings in ppm vs. monomer; $[BA]_0$ = 4.5 M.

An interesting point to note is that, according to the kinetic plots presented in **Figure 7A** and PREDICI simulations provided in the **SI**, bimolecular radical termination (RT) should dominate catalytic radical termination (CRT), contrary to previous studies with other ATRP catalysts.[13] If CRT would significantly contribute to overall termination, the polymerization kinetics would depend on catalyst concentration (**Eq. 6**), where k_{CRT}^{app} is the apparent CRT rate coefficient.[73] This is because, as shown in **Scheme 3**, CRT requires the coordination of a propagating radical ($P_n^{\bullet}$) to the L/Cu^{I} complex to form a L/Cu^{II}-P_n organometallic species.[73]

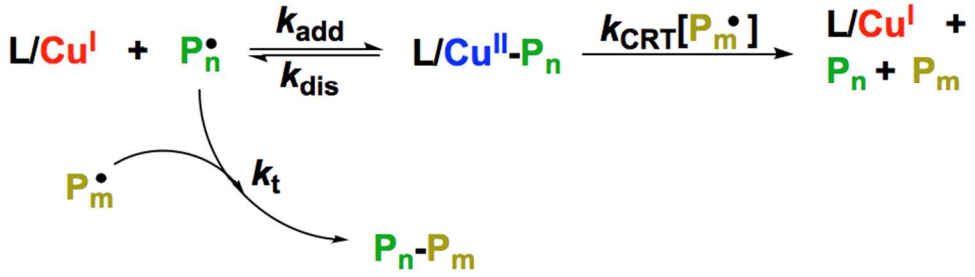

Scheme 3 Interplay between conventional bimolecular radical termination (RT) and catalytic radical termination via the reactive L/Cu^{II}-P_n intermediate in ATRP of acrylates.

Since the L/Cu^{I} concentration in ICAR ATRP is governed by the dynamic ATRP equilibrium[74] (**Scheme 1**), and considering the very high values of $K_{ATRP} \approx 10^{-1}$ for this system, the amount of TPMA^{NMe2}/Cu^{I} present in solution is calculated to be 9.6 x 10^{-10} at equilibrium (See **Supporting Information** for calculation).[74] In other words, a radical will kinetically terminate with a second radical faster than with the trace amounts of TPMA^{NMe2}/Cu^{I}. This should still happen, even if addition of a radical to TPMA^{NMe2}/Cu^{I} occurs at diffusion controlled rates (k_{add} = 10^{8} $M^{-1}s^{-1}$). This is not the case of less active catalysts such as TPMA-based systems ($K_{ATRP} \approx 10^{-5}$)[63] where CRT dominates because of a relatively higher concentration of TPMA/Cu^{I} of 1.8 x 10^{-6} M. As shown in **Figure S10**, these findings are supported by PREDICI simulations: the much more active TPMA^{NMe2}-based system kinetically suppressed CRT because only a small fraction of TPMA^{NMe2}/Cu^{I} is present in solution, resulting in a relatively larger fraction of living chains compared to less active systems.

Then, Ag^{0} ATRP, a form of ARGET ATRP, was conducted to further test the scope of the newly synthesized catalyst. Ag^{0} ATRP employs silver wire to heterogeneously reduce L/Cu^{II} to

L/Cu^{I}, with oxidation of Ag^{0} to Ag^{I}Br.[11] As shown in **Figure 8**, the TPMA^{NMe2} catalyst successfully polymerized MA via Ag^{0} ARGET ATRP using as little as 10 ppm of catalyst relative to monomer. However, at 5 ppm, the polymerization was no longer living as confirmed by the molecular weights decreasing with conversion and high *Đ* values (>1.5). Since the rate of Ag^{0} ARGET ATRP depends on the rate of Cu^{I} generation, the linear semi-logarithmic kinetic plots showed that Cu^{II} was still reduced but unable to efficiently deactivate radicals. This is because, at such low catalyst concentrations, the rate of propagation and termination are competing with the rate of deactivation. Thus, it is likely that 10 ppm is around the lowest possible limits to achieve a well-controlled polymerization in copper catalyzed ATRP of acrylates. Nevertheless, unprecedented control was achieved using as little as 10 ppm of catalyst for the polymerization of acrylates. The nearly colorless nature of the polymerization solution at 10 ppm can be seen in **Figure 8C**.

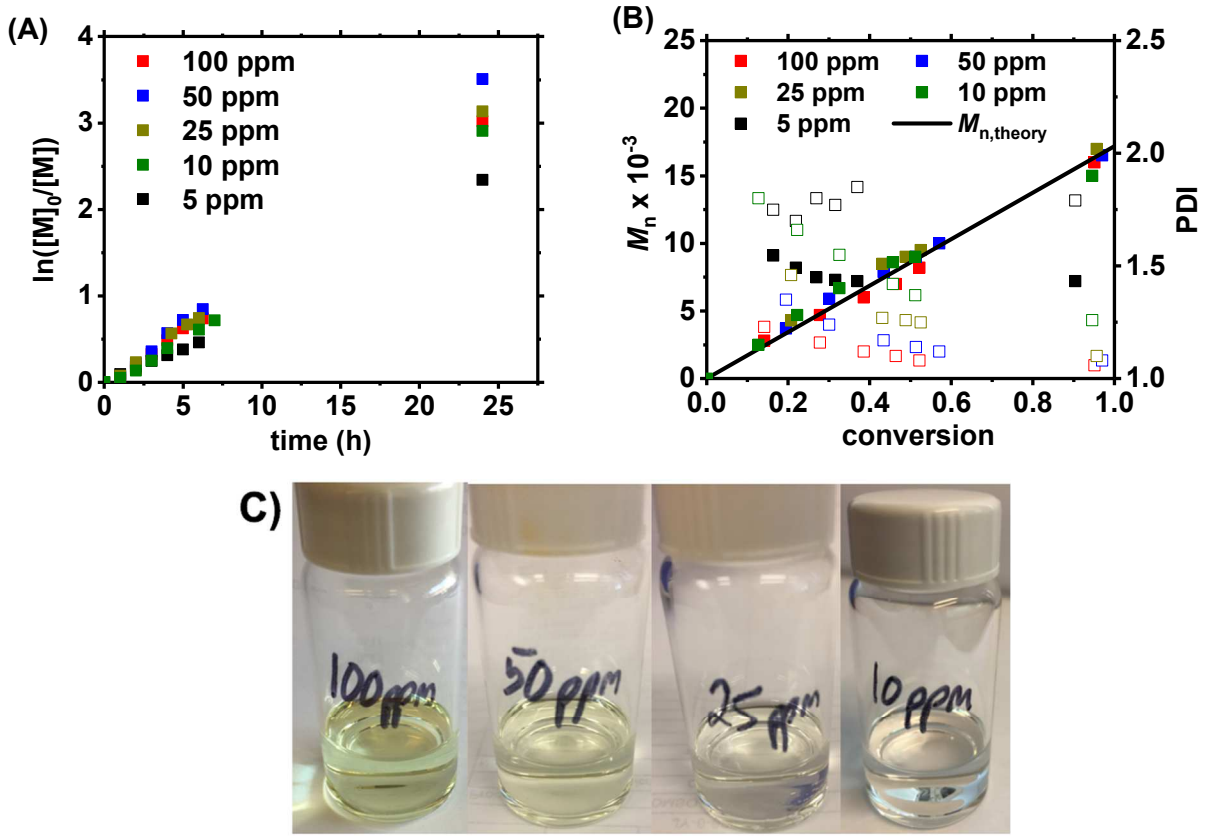

Figure 8 A) Semi-logarithmic plots and B) M_n and *Đ* vs. conversion for the Ag^{0} ATRP of methyl acrylate (MA) at different loadings of [Cu^{II}(TPMA^{NMe2})Br][Br] under the initial conditions [MA]$_0$:[EBiB]$_0$:[Cu^{II}(TPMA^{NMe2})Br][Br]$_0$ = 200:1:0.02-0.002 with 10 cm Ag^{0} wire (SA/V) = 0.53 cm^{-1} in DMF at 50 °C; catalyst loadings in ppm vs. monomer; [MA]$_0$ = 5.75M and C) pictures of polymerization solution at decreasing catalyst loadings of [Cu^{II}(TPMA^{NMe2})Br][Br].

Using the results from the two polymerization systems shown in **Figures 6 & 7**, one can estimate the rate coefficient of deactivation, k_d, according to **Eq 7** where DP is the degree of polymerization, k_p is the propagation rate constant,[75] and p is monomer conversion.[4]

$$M_w / M_n = 1 + \frac{1}{DP} + \left(\frac{k_p[RX]}{k_d[LCu^{II} - X]} \right) \left(\frac{2}{p} - 1 \right) \quad \textbf{(Eq. 7)}$$

Due to the negligible amount of termination, it has been assumed that $[RX] = [RX]_0$. Furthermore, since the K_{ATRP} is so large, it can be assumed that essentially all copper is in the form of L/Cu^{II}-X and therefore $[L/Cu^{II}\text{-}X] = [L/Cu^{II}\text{-}X]_0$. Using the final dispersity data of the polymerizations in **Figures 6 & 8**, $k_d = (5.4 \pm 1.7) \times 10^7$ M^{-1}s^{-1} was obtained which gives an estimated value of $K_{ATRP} = 2.2 \times 10^{-2}$ for acrylate systems. This indicates that the degree of substitution and redox potential of pyridinic-based catalysts have very little effect on k_d. Instead, only the total amount of Cu^{II}-X deactivator, which is regulated by $[Cu^{II}]_0$ and K_{ATRP}, will define the level of control in a particular ATRP system with activator regeneration.

Comparison of TPMA^{NMe2} to Other Ligands in ATRP

As shown in **Figure 8**, the redox potential scales linearly with log(K_{ATRP}) for EBiB in MeCN at room temperature for a variety of ligands (**Figure S11** for structures of ligands). Based on $E_{1/2}$ values, the newly synthesized TPMA^{NMe2}-based catalyst ($E_{1/2}$ = -554 mV) is almost 10 billion times more active than seminal bpy-based catalyst ($E_{1/2}$ = +30 mV). Even looking at catalysts which are widely used for low ppm ATRP, the TPMA^{NMe2}-based system is ≈300,000 and 30,000 times more active than the TPMA ($E_{1/2}$ = -240 mV) and Me$_6$TREN ($E_{1/2}$ = -300 mV) based catalysts, respectively. Unfortunately, with such a highly active catalyst as [Cu(TPMA^{NMe2})]$^+$, activation of alkyl halides approaches diffusion controlled limits (k_a >10^6 M^{-1}s^{-1}), and with already diffusion controlled deactivation rates (k_d = >10^7 M^{-1}s^{-1}), values of K_{ATRP} begin to approach unity. This would mean that for commonly used monomers such as acrylates and methacrylates, this catalytic system may be the upper limit of activity since the only way to

further increase K_{ATRP} would be to decrease k_d. This is not best since the control achieved in ATRP is due to fast rates of deactivation. Encouragingly, the high ATRP activity provided by the $TPMA^{NMe2}$-based catalyst can open the possibility to polymerize less active monomers such as vinyl acetate and *N*-vinylpyrrolidone which have historically fallen victim to too low values of K_{ATRP}.

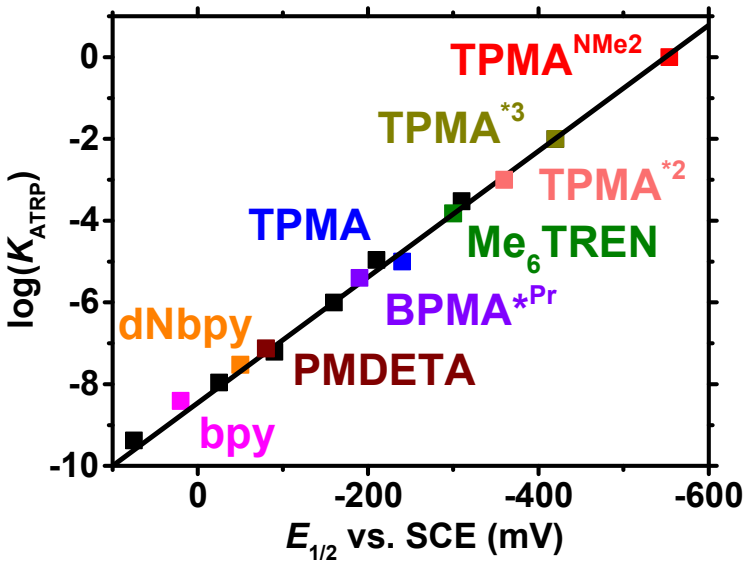

Figure 9 Redox potential ($E_{1/2}$) vs. log(K_{ATRP}) for various ATRP catalysts complexed by multidentate nitrogen-based ligands. Values for $E_{1/2}$ have previously been determined experimentally vs. an SCE electrode in MeCN at room temperature. Values of K_{ATRP} are for ethyl α-bromoisobutyrate (EBiB; methacrylate mimic) in MeCN at room temperature. Structures of all ligands are shown in **Figure S11**.

Conclusions

The synthesis of a new ATRP catalyst employing the p-dimethylamino substituted TPMA ligand, tris[(4-dimethylaminiopyridyl)methyl]amine ($TPMA^{NMe2}$), is reported. Variable temperature NMR showed a fluxional Cu^{I} complex with rapid ligand exchange. In the solid state, the $[Cu^{II}(TPMA^{NMe2})Br]^{+}$ complex exhibited nearly perfect trigonal bipyramidal geometry. UV-Vis and EPR confirmed that this geometry was retained in solution. Electrochemical measurements showed a quasi-reversible $TPMA^{NMe2}Cu^{I/II}$ couple indicating small geometric rearrangement throughout the redox cycle. Stability constants for Cu^{I} and Cu^{II} were comparable to other copper ATRP catalysts in MeCN. Electrochemistry was also utilized to assess the activation of methyl 2-bromopropionate (MBrP; acrylate mimic) and ethyl α-

bromoisobutyrate, for which a rate coefficient of activation was measured as k_a = 1.1 x 10^6 $M^{-1}s^{-1}$ and 7.2 x 10^6 $M^{-1}s^{-1}$, respectively. This leads to an estimation of K_{ATRP} = 2.2 x10^{-2} and 7.2 x10^{-1}, respectively which indicated this is the most active ATRP catalyst to date. A large value of k_d > 10^7 M^{-1} s^{-1} was calculated and indicated that the catalyst is also a good deactivator. Both ICAR and Ag^0 ATRP of acrylates were well-controlled using as little as 10 ppm of catalyst relative to monomer. Encouragingly, due to the high values of K_{ATRP} and low [$TPMA^{NMe2}$/Cu^I], unwanted side reactions involving Cu^I such as catalytic radical termination (CRT) are suppressed leading to higher chain-end functionality. Furthermore, this catalyst can potentially allow for the successful ATRP of less active monomers. Investigations in this direction are currently ongoing in our laboratories.

ASSOCIATED CONTENT

Supporting Information

Experimental procedures, X-ray diffraction details, discussion of electrochemical methods, GPC traces, example calculations of L/Cu^I at steady-state, kinetic simulations and structures of common ligands employed in ATRP.

AUTHOR INFORMATION

Corresponding Author:

*(K.M.) Email: km3b@andrew.cmu.edu

◊T.R. and M.F. contributed equally.

Notes

The authors declare no competing financial interest.

ACKNOWLEDGEMENTS

Support from the NSF (CHE 1707490) is acknowledged. We thank the Centre National de la Recherche Scientifique (CNRS) for support through the PICS06782 grant and through the Laboratoire International Associé (LIA) “Laboratory of Coordination Chemistry for Controlled Radical Polymerization”. We are also grateful to the French Embassy in Washington D.C. for a

Chateaubriand Fellowship to T.R. We would like to acknowledge Mateusz Olszewski for designing the graphical abstract for this manuscript.

REFERENCES

1. Matyjaszewski, K.; Xia, J. *Chemical Reviews* **2001,** *101* (9), 2921-2990.
2. Wang, J.-S.; Matyjaszewski, K. *Journal of the American Chemical Society* **1995,** *117* (20), 5614-5615.
3. Kato, M.; Kamigaito, M.; Sawamoto, M.; Higashimura, T. *Macromolecules* **1995,** *28* (5), 1721-1723.
4. Matyjaszewski, K. *Macromolecules* **2012,** *45* (10), 4015-4039.
5. Wang, J.-S.; Matyjaszewski, K. *Macromolecules* **1995,** *28* (23), 7901-7910.
6. Matyjaszewski, K.; Tsarevsky, N. V. *Journal of the American Chemical Society* **2014,** *136* (18), 6513-6533.
7. Matyjaszewski, K.; Jakubowski, W.; Min, K.; Tang, W.; Huang, J.; Braunecker, W. A.; Tsarevsky, N. V. *Proceedings of the National Academy of Sciences* **2006,** *103* (42), 15309-15314.
8. Konkolewicz, D.; Magenau, A. J. D.; Averick, S. E.; Simakova, A.; He, H.; Matyjaszewski, K. *Macromolecules* **2012,** *45* (11), 4461-4468.
9. Chan, N.; Cunningham, M. F.; Hutchinson, R. A. *Macromolecular Chemistry and Physics* **2008,** *209* (17), 1797-1805.
10. Jakubowski, W.; Matyjaszewski, K. *Angewandte Chemie* **2006,** *118* (27), 4594-4598.
11. Williams, V. A.; Ribelli, T. G.; Chmielarz, P.; Park, S.; Matyjaszewski, K. *Journal of the American Chemical Society* **2015,** *137* (4), 1428-1431.
12. Konkolewicz, D.; Wang, Y.; Zhong, M.; Krys, P.; Isse, A. A.; Gennaro, A.; Matyjaszewski, K. *Macromolecules* **2013,** *46* (22), 8749-8772.
13. Ribelli, T. G.; Konkolewicz, D.; Bernhard, S.; Matyjaszewski, K. *Journal of the American Chemical Society* **2014,** *136* (38), 13303-13312.
14. Pan, X.; Tasdelen, M. A.; Laun, J.; Junkers, T.; Yagci, Y.; Matyjaszewski, K. *Progress in Polymer Science* **2016,** *62*, 73-125.
15. Anastasaki, A.; Nikolaou, V.; Zhang, Q.; Burns, J.; Samanta, S. R.; Waldron, C.; Haddleton, A. J.; McHale, R.; Fox, D.; Percec, V.; Wilson, P.; Haddleton, D. M. *Journal of the American Chemical Society* **2014,** *136* (3), 1141-1149.
16. Discekici, E. H.; Anastasaki, A.; Kaminker, R.; Willenbacher, J.; Truong, N. P.; Fleischmann, C.; Oschmann, B.; Lunn, D. J.; Read de Alaniz, J.; Davis, T. P.; Bates, C. M.; Hawker, C. J. *Journal of the American Chemical Society* **2017,** *139* (16), 5939-5945.
17. Anastasaki, A.; Oschmann, B.; Willenbacher, J.; Melker, A.; Van Son, M. H. C.; Truong, N. P.; Schulze, M. W.; Discekici, E. H.; McGrath, A. J.; Davis, T. P.; Bates, C. M.; Hawker, C. J. *Angewandte Chemie International Edition* **2017,** *56* (46), 14483-14487.
18. Chmielarz, P.; Fantin, M.; Park, S.; Isse, A. A.; Gennaro, A.; Magenau, A. J. D.; Sobkowiak, A.; Matyjaszewski, K. *Progress in Polymer Science* **2017,** *69*, 47-78.
19. Wang, Z.; Pan, X.; Li, L.; Fantin, M.; Yan, J.; Wang, Z.; Wang, Z.; Xia, H.; Matyjaszewski, K. *Macromolecules* **2017,** *50* (20), 7940-7948.
20. Mohapatra, H.; Kleiman, M.; Esser-Kahn, A. P. *Nat Chem* **2017,** *9* (2), 135-139.

21. Lin, C. Y.; Coote, M. L.; Gennaro, A.; Matyjaszewski, K. *Journal of the American Chemical Society* **2008,** *130* (38), 12762-12774.
22. Coessens, V.; Pintauer, T.; Matyjaszewski, K. *Progress in Polymer Science* **2001,** *26* (3), 337-377.
23. Tang, W.; Tsarevsky, N. V.; Matyjaszewski, K. *Journal of the American Chemical Society* **2006,** *128* (5), 1598-1604.
24. Tsarevsky, N. V.; Braunecker, W. A.; Tang, W.; Matyjaszewski, K. *ACS Symposium Series* **2009,** *1023* (Controlled/Living Radical Polymerization: Progress in ATRP), 85-96.
25. Braunecker, W. A.; Tsarevsky, N. V.; Gennaro, A.; Matyjaszewski, K. *Macromolecules* **2009,** *42* (17), 6348-6360.
26. Tang, W.; Kwak, Y.; Braunecker, W.; Tsarevsky, N. V.; Coote, M. L.; Matyjaszewski, K. *Journal of the American Chemical Society* **2008,** *130* (32), 10702-10713.
27. Gillies, M. B.; Matyjaszewski, K.; Norrby, P.-O.; Pintauer, T.; Poli, R.; Richard, P. *Macromolecules* **2003,** *36* (22), 8551-8559.
28. Tang, W.; Matyjaszewski, K. *Macromolecules* **2006,** *39* (15), 4953-4959.
29. Tsarevsky, N. V.; Braunecker, W. A.; Vacca, A.; Gans, P.; Matyjaszewski, K. *Macromolecular Symposia* **2007,** *248* (1), 60-70.
30. Rorabacher, D. B. *Chemical Reviews* **2004,** *104* (2), 651-698.
31. Schroder, K.; Mathers, R. T.; Buback, J.; Konkolewicz, D.; Magenau, A. J. D.; Matyjaszewski, K. *ACS Macro Letters* **2012,** *1* (8), 1037-1040.
32. Lee, J. Y.; Peterson, R. L.; Ohkubo, K.; Garcia-Bosch, I.; Himes, R. A.; Woertink, J.; Moore, C. D.; Solomon, E. I.; Fukuzumi, S.; Karlin, K. D. *Journal of the American Chemical Society* **2014,** *136* (28), 9925-9937.
33. Magenau, A. J. D.; Kwak, Y.; Schröder, K.; Matyjaszewski, K. *ACS Macro Letters* **2012,** *1* (4), 508-512.
34. Zhang, C. X.; Kaderli, S.; Costas, M.; Kim, E.-i.; Neuhold, Y.-M.; Karlin, K. D.; Zuberbühler, A. D. *Inorganic Chemistry* **2003,** *42* (6), 1807-1824.
35. Comba, P.; Morgen, M.; Wadepohl, H. *Inorganic Chemistry* **2013,** *52* (11), 6481-6501.
36. Kim, S.; Lee, J. Y.; Cowley, R. E.; Ginsbach, J. W.; Siegler, M. A.; Solomon, E. I.; Karlin, K. D. *Journal of the American Chemical Society* **2015,** *137* (8), 2796-2799.
37. Solomon, E. I.; Sundaram, U. M.; Machonkin, T. E. *Chemical Reviews* **1996,** *96* (7), 2563-2606.
38. Solomon, E. I.; Heppner, D. E.; Johnston, E. M.; Ginsbach, J. W.; Cirera, J.; Qayyum, M.; Kieber-Emmons, M. T.; Kjaergaard, C. H.; Hadt, R. G.; Tian, L. *Chemical Reviews* **2014,** *114* (7), 3659-3853.
39. Wilmot, C. M.; Hajdu, J.; McPherson, M. J.; Knowles, P. F.; Phillips, S. E. V. *Science* **1999,** *286* (5445), 1724-1728.
40. Solomon, E. I.; Chen, P.; Metz, M.; Lee, S.-K.; Palmer, A. E. *Angewandte Chemie International Edition* **2001,** *40* (24), 4570-4590.
41. Decker, H.; Dillinger, R.; Tuczek, F. *Angewandte Chemie International Edition* **2000,** *39* (9), 1591-1595.
42. Fry, H. C.; Lucas, H. R.; Narducci Sarjeant, A. A.; Karlin, K. D.; Meyer, G. J. *Inorganic Chemistry* **2008,** *47* (1), 241-256.
43. Kaur, A.; Ribelli, T. G.; Schröder, K.; Matyjaszewski, K.; Pintauer, T. *Inorganic Chemistry* **2015,** *54* (4), 1474-1486.

44. Wang, Y.; Zhong, M.; Zhu, W.; Peng, C.-H.; Zhang, Y.; Konkolewicz, D.; Bortolamei, N.; Isse, A. A.; Gennaro, A.; Matyjaszewski, K. *Macromolecules* **2013,** *46* (10), 3793-3802.
45. Mason, J. *Chemical Reviews* **1987,** *87* (6), 1299-1312.
46. Eckenhoff, W. T.; Garrity, S. T.; Pintauer, T. *European Journal of Inorganic Chemistry* **2008,** *2008* (4), 563-571.
47. Hsu, S. C. N.; Chien, S. S. C.; Chen, H. H. Z.; Chiang, M. Y. *Journal of the Chinese Chemical Society* **2007,** *54* (3), 685-692.
48. Kitagawa, S.; Munakata, M. *Inorganic Chemistry* **1981,** *20* (7), 2261-2267.
49. Kitagawa, S.; Munakata, M.; Miyaji, N. *Inorganic Chemistry* **1982,** *21* (10), 3842-3843.
50. Munakata, M.; Kitagawa, S.; Kosome, S.; Asahara, A. *Inorganic Chemistry* **1986,** *25* (15), 2622-2627.
51. Thompson, J. S.; Swiatek, R. M. *Inorganic Chemistry* **1985,** *24* (1), 110-113.
52. Eckenhoff, W. T.; Pintauer, T. *Inorganic Chemistry* **2010,** *49* (22), 10617-10626.
53. Zerk, T. J.; Bernhardt, P. V. *Coordination Chemistry Reviews*.
54. Hiskey, M. A.; Ruminski, R. R. *Inorganica Chimica Acta* **1986,** *112* (2), 189-195.
55. McLachlan, G. A.; Fallon, G. D.; Martin, R. L.; Spiccia, L. *Inorganic Chemistry* **1995,** *34* (1), 254-261.
56. Pintauer, T.; Qiu, J.; Kickelbick, G.; Matyjaszewski, K. *Inorganic Chemistry* **2001,** *40* (12), 2818-2824.
57. Zerk, T. J.; Bernhardt, P. V. *Inorganic Chemistry* **2017,** *56* (10), 5784-5792.
58. Bortolamei, N.; Isse, A. A.; Di Marco, V. B.; Gennaro, A.; Matyjaszewski, K. *Macromolecules* **2010,** *43* (22), 9257-9267.
59. De Paoli, P.; Isse, A. A.; Bortolamei, N.; Gennaro, A. *Chemical Communications* **2011,** *47* (12), 3580-3582.
60. Qiu, J.; Matyjaszewski, K.; Thouin, L.; Amatore, C. *Macromolecular Chemistry and Physics* **2000,** *201* (14), 1625-1631.
61. S. Ahrland, K. N., B Tagesson *Acta Chemica Scandinavica A* **1983,** *37*, 193-201.
62. Gritzner, G. *The Journal of Physical Chemistry* **1986,** *90* (21), 5478-5485.
63. Ribelli, T. G.; Augustine, K. F.; Fantin, M.; Krys, P.; Poli, R.; Matyjaszewski, K. *Macromolecules* **2017,** *50* (20), 7920-7929.
64. Fantin, M.; Isse, A. A.; Matyjaszewski, K.; Gennaro, A. *Macromolecules* **2017,** *50* (7), 2696-2705.
65. Bell, C. A.; Bernhardt, P. V.; Monteiro, M. J. *Journal of the American Chemical Society* **2011,** *133* (31), 11944-11947.
66. Marco Fantin, F. L., Armando Gennaro, Abdirisak A. Isse, Krzysztof Matyjaszewski *Synthesis* **2017,** *49* (15), 2211-3322.
67. Bortolamei, N.; Isse, A. A.; Magenau, A. J. D.; Gennaro, A.; Matyjaszewski, K. *Angewandte Chemie International Edition* **2011,** *50* (48), 11391-11394.
68. Fantin, M.; Isse, A. A.; Gennaro, A.; Matyjaszewski, K. *Macromolecules* **2015,** *48* (19), 6862-6875.
69. Savéant, J. M.; Su, K. B. *Journal of Electroanalytical Chemistry and Interfacial Electrochemistry* **1984,** *171* (1), 341-349.
70. D'Hooge, D. R.; Konkolewicz, D.; Reyniers, M.-F.; Marin, G. B.; Matyjaszewski, K. *Macromolecular Theory and Simulations* **2012,** *21* (1), 52-69.
71. Ribelli, T. G.; Konkolewicz, D.; Pan, X.; Matyjaszewski, K. *Macromolecules* **2014,** *47* (18), 6316-6321.

72. Krys, P.; Matyjaszewski, K. *European Polymer Journal* **2017,** *89*, 482-523.
73. Ribelli, T. G.; Wahidur Rahaman, S. M.; Daran, J.-C.; Krys, P.; Matyjaszewski, K.; Poli, R. *Macromolecules* **2016,** *49* (20), 7749-7757.
74. Krys, P.; Ribelli, T. G.; Matyjaszewski, K.; Gennaro, A. *Macromolecules* **2016,** *49* (7), 2467-2476.
75. Barner-Kowollik, C.; Beuermann, S.; Buback, M.; Castignolles, P.; Charleux, B.; Coote, M. L.; Hutchinson, R. A.; Junkers, T.; Lacik, I.; Russell, G. T.; Stach, M.; van Herk, A. M. *Polymer Chemistry* **2014,** *5* (1), 204-212.

For Table of Contents Use Only